



Adsorption of a cationic dye from aqueous solution on mesoporous carbon-based honeycomb monolith

Soraya Hosseini^a, Thomas S.Y. Choong^{a,b,*}, Muhammad Hamid^{a,c}

^aDepartment of Chemical and Environmental Engineering, Universiti Putra Malaysia, 43400 UPM Serdang, Selangor, Malaysia

^bINTROP, Universiti Putra Malaysia, 43400 UPM Serdang, Selangor, Malaysia
Tel. +60 389466293; Fax: +60 386567120; email: tsyc2@eng.upm.edu.my

^cFaculty of Engineering, Department of Chemical Engineering, Malikussaleh University, Lhokseumawe–Aceh, Indonesia

Received 4 August 2011; Accepted 9 July 2012

ABSTRACT

A carbon-based honeycomb monolith was prepared using dip-coating method. The carbon-based monolith was then used to remove a cationic dye (methylene blue [MB]) from aqueous solution. Surface chemistry studies demonstrated that acidic functionality ($0.567 \text{ mmol g}^{-1}$) dominated as compared to basic functionality ($0.019 \text{ mmol g}^{-1}$). N_2 adsorption/desorption revealed a mesoporous structure. The Brunauer-Emmett-Teller surface area was approximately $352 \text{ m}^2 \text{ g}^{-1}$ and the mesoporous volume devoted about 67% the total pore volume. The effects of different parameters (such as initial pH, initial dye concentration, temperature, and contact time) on MB removal were investigated in batch mode. The maximum adsorption capacity is around 121.3 mg g^{-1} at optimum $\text{pH} = 10$. An increase in adsorption capacity was observed via increasing MB concentration, with equilibration time ranged between 3,200 and 4,000 min. Both the Langmuir and the Redlich-Peterson models were found to describe well the equilibrium data. Kinetic studies showed better fitting for the pseudo-second-order model. The intraparticle diffusion model showed multilinearity, indicating two or more steps were involved to describe the adsorption process. Regeneration studies showed that the adsorption capacity of the adsorbent was reduced by about 20% after six cycles.

Keywords: Adsorption; Honeycomb; Monolith; Mesoporous carbon; Methylene blue

1. Introduction

Due to increasing of toxic pollutants in the environment and demand for natural water, research activities have focused on the development of new techniques for pollutant removal from wastewater [1,2]. Since dyes are recalcitrant organic molecules, resistant to aerobic digestion, and stable to light and oxidizing solutions, different techniques were applied for treatment of dyes solutions [3,4]. Adsorption is

one of the effective methods for wastewater treatment as compared to other techniques in terms of initial cost, flexibility, and simplicity of design [5–11]. Activated carbon has been traditionally known for dyes removal in wastewater treatment [12].

Separation and regeneration are major problems of activated carbon powder [13]. Mesoporous carbonic materials are well known due to their ability to adsorb large molecules, thus, much attention was focused on preparing mesoporous carbons by sol-gel method, carbonization, and activation of carbon precursors and template method using surfactants [14,15]. A thin layer of carbon can be coated on a suitable ceramic

*Corresponding author.

carrier (cordierite honeycombs), which are themselves mechanically strong in nature. Honeycomb monolith is used as a support due to its commercial availability, low thermal expansion coefficient, low pressure drop, relatively uniform porosity, easy regeneration, high mechanical strength, and excellent thermal stability [16,17]. Carbonic materials can be made from a variety of materials, including natural source (wood, coconut shell, etc.) and synthetic source (furfuryl alcohol, phloroglucinol, resorcinol, furan resin, phenolic resin, novolac, cellulose, and polysaccharides) [18]. Poly furfuryl alcohol, a thermosetting resin, gives high carbon yield and is therefore, a suitable carbon source for coating monolithic supports.

Methylene blue (MB) is widely used in dyeing cottons, wool, hair colorant, and paper. It is thus selected here to investigate the adsorption properties of carbon-coated monolith for a cationic dye [19]. Very few studies on adsorption using mesoporous-activated carbon-coated monolith have been reported. In the previous work, methyl orange (an anionic dye) adsorption on carbon-coated monolith was carried out at optimum pH=6 [20]. The present work aims to examine in detail the behavior of carbon-coated monolith as an adsorbent for the adsorption of MB from aqueous solution. For adsorption of large molecules, high mesoporosity is desired. The effects of contact time, initial dye concentration, and pH on MB adsorption were studied on a batch mode.

2. Experimental method

2.1. Preparation and characterization of adsorbent

Cordierite monolith (circular cross-section with square channel) used was of 400 cells per square inch with specifications of channel width 1.02 ± 0.02 mm, and wall thickness 0.25 ± 0.02 mm. The cordierite monolith is of 2.5 ± 0.02 mm diameter and 2.5 ± 0.02 mm length. The cordierite monoliths were purchased from Beihai Haihuang Chemical Packing Co. Ltd, China. The chemical compositions of monolithic substrate are SiO₂ $50.9 \pm 1\%$, Al₂O₃ $35.2 \pm 1\%$, MgO $13.9 \pm 0.5\%$, and others <1%. The mesoporous carbon was synthesized by polymerization of furfuryl alcohol (99%), polyethylene glycol (PEG 8000), pyrrole (99%), and nitric acid (65%). Furfuryl alcohol as a carbon source is polymerized by using nitric acid (HNO₃) as the catalyst. The polymerization of furfuryl alcohol produced poly furfuryl alcohol and water. Polyethylene glycol was added as a pore former and pyrrole as a binder [21,22].

A partially polymerized furfuryl alcohol mixture was used as dip-coating liquid to obtain a polymer-coated monolithic support. The polymerization

catalyst (nitric acid) was added stepwise every 5 min, 0.25 mL each time, into the mixture for 1 h while temperature was maintained at approximately 20°C. The bare monolith was dried in an oven at temperature 120°C. The dried monolith was immersed in the polymer solution for 20 min. The excess coating solution was removed from monolith channel by blowing pressurized air. This polymer was converted into carbon by thermal treatment in an inert atmosphere. The light brown monolith was heated at temperature $110 \pm 2^\circ\text{C}$ for 24 h. The samples were carbonized at 650°C for 2 h in flowing N₂ and heating rate of $10^\circ\text{C min}^{-1}$. Activation process was performed at 400°C by flowing argon gas with 5% oxygen for 4 h.

Surface characteristics of adsorbent, including specific surface area and pore size distribution, were measured by physical adsorption/desorption of N₂ gas using a Sorptomatic V1.03 micropore analyzer. The Brunauer-Emmett-Teller (BET) method is widely used for the calculation of the surface area. The sample (approximately 0.1 g) was first outgassed under high vacuum for 12 h at 250°C. The sample was then cooled to 30°C. The temperature of system was kept constant by immersing the sample tube in a bath of liquid nitrogen (-195.6°C), and subjected to a range of pressures, to generate adsorption/desorption isotherms. To identify the surface functional groups, Fourier transform infrared (FTIR) analysis was carried out. The carbon-coated monolith was grinded using mortar and pestle to make fine powder. For FTIR measurement, a small amount of sample was added to KBr powder. Infrared spectra were obtained by scanning the prepared sample with a spectrometer (Perkin 100). Dry air was continuously purged into the spectrometer to get rid of water vapor. The sample was scanned in the range of $4,000\text{--}400\text{ cm}^{-1}$. A plot of infrared radiation intensity vs. wave number known as the infrared spectrum was recorded for samples. Scanning electron microscopy (SEM) was carried out using an electron microscope system (LEO 1450VP) for surface morphology analysis of mesoporous carbon-coated monolith.

2.2. MB adsorption

MB (C.I. 52,015, 319.85 g mol^{-1} , C₁₆H₁₈N₃ClS, cationic dye) was used as the pollutant without further purification. Distilled water was used throughout all experiments and in the preparation of solution. A stock solution of MB concentration 1,000 ppm (pH=3.3) was prepared by dissolving 1 g dye powder in 1 L of distilled water (pH ~7). The MB absorbance wavelength of the residual concentration was determined by a UV-visible spectrophotometer (Ultrospec™ 3100p) at $\lambda_{\text{max}} = 664\text{ nm}$. The batch mode

adsorption was carried out by immersing one piece of monolith (amount of carbon 0.7 g) in 250 mL of dye solution. The dye solution was continuously stirred in a shaking bath with a speed of 150 rpm at 30°C until equilibrium was reached.

Kinetic and isotherm experiments were carried out with initial MB concentration in the range from 50 to 480 ppm. The residual concentration of dye solution was measured immediately to reduce errors due to dye adsorption onto glassware. Samples of 0.1 mL dye solution were drawn at time interval 5 min for 60 min and after that every 60 min until equilibrium. Experiments were carried out twice, and the values were reported with average error ($\pm 3\%$). The amount of pollutant adsorbed at any time, q_t (mg g^{-1}), was calculated by Eq. (1):

$$q_t = \frac{(C_0 - C_t)V}{m} \quad (1)$$

where C_0 and C_t (mg L^{-1}) are the concentrations of dye at initial time ($t=0$) and at any time (t), respectively, V is the volume of the solution (L) and m is the mass of carbon (g).

2.3. Determination of optimum pH, point zero charge and surface chemistry

The effect of solution pH on the removal of MB was investigated by varying pH from 2 to 10, with initial concentration of 100 ppm. The adsorption was performed at room temperature. The pH was adjusted using HCl (0.5 N) and NaOH (0.5 N). The study was carried out by immersing one piece of monolith (amount of carbon ~ 0.7 g) in 250 mL of dye solution, stirred in a shaker at 150 rpm and the final concentration was recorded after 48 h. The adsorption capacity was calculated to determine the optimum pH.

The pH of zero point charge (pH_{pzc}) of carbon-coated monolith was determined by the solid addition procedure [23]. The net charge of surface is zero on the adsorbent surface at pH_{pzc} . Therefore, no activation of acidic or basic functional groups is detected on the solution pH. Carbon-coated monolith (0.7 g carbon) was added to nine flasks with an individual pH (2–10), including 100 mL solution KNO_3 (0.01 N). The initial pH of solutions was adjusted by adding KOH (0.5 N) and HNO_3 (0.5 N) solutions. Each flask was immediately sealed with parafilm and shaken thoroughly at 30°C for 48 h. The amount of charge on carbon-coated monolith was calculated by ΔpH (the difference between the initial pH and the final pH). The intersection of the obtained curve with pH_0 axis indicated the pH_{pzc} value. To confirm the point of pH_{pzc} , the experi-

ments were repeated by NaCl (0.01 N) with pH adjusted using NaOH (0.5 N) and HCl (0.5 N).

The amount of surface acidic and basic functional groups was determined using the Boehm titration method [24]. The carbon samples were immersed into 50 mL HCl (0.1 N), NaHCO_3 (0.1 N), Na_2CO_3 (0.1 N), and NaOH (0.1 N) solutions and were shaken for 72 h. The suspension was then centrifuged at 5,000 rpm for 5 min. Each solution (10 mL) was pipetted and the excess of base was titrated with HCl (0.1 N). The surface basic sites were calculated from the amount of HCl that was reacted with the carbon.

2.4. Regeneration studies

Desorption was carried out in batch mode. The carbon coated monolith (CCM) (0.7 g) was initially saturated with MB solution of 250 mL with initial concentration 400 ppm. After equilibration, the unadsorbed traces of MB were removed via washing several times the adsorbent with distilled water. The desorption process was carried out using HCl solution of 0.5 M. The CCM was then washed with distilled water to remove excessive acidity. After that the CCM was again utilized to treat MB solution. This procedure continued for several cycles.

3. Results and discussion

3.1. Characterization of adsorbents

The surface area and the pore volume were determined using N_2 adsorption/desorption isotherms. The total surface area and the volume of micropores were calculated by BET equation and t -plot in the relative pressure $P/P^0 = 0.995$. N_2 adsorption/desorption isotherm of carbon-coated monolith at 77 K gives a type IV isotherm according to the IUPAC classification, indicating a mesoporous system. The textural parameters are summarized in Table 1.

The mesoporous volume can be calculated by taking the difference of total volume and micropore volume. The BET analysis revealed that around 82% of the total surface area is mesoporous, while 67% of the total pore volume is in the mesoporous range. The pore size distribution curve is shown in Fig. 1. Surface morphology, closely related to apparent porosity of mesoporous carbon coated is revealed in Fig. 2. The image of a carbon-coated monolith taken at a magnification of 20.0 kX shows highly dense and irregular surface. These irregular pores were resulted from the decomposition of PEG in the mesoporous carbon prior to carbonization process. Fig. 3 shows SEM image of bare monolith, demonstrating a smooth surface.

Table 1
Textural parameters and active sites of carbon-coated monolith

Parameter	Value
BET area ($\text{m}^2 \text{g}^{-1}$)	352
Mesopores area ($\text{m}^2 \text{g}^{-1}$)	288
Micropore ($\text{m}^2 \text{g}^{-1}$)	64
Total pore volume ($\text{cm}^3 \text{g}^{-1}$)	0.25
Mesopore volume ($\text{cm}^3 \text{g}^{-1}$)	0.17
Micropore volume ($\text{cm}^3 \text{g}^{-1}$)	0.08
Carboxylic (mmol g^{-1})	0.159
Lactonic (mmol g^{-1})	0.008
Phenolic (mmol g^{-1})	0.400
Acidity (mmol g^{-1})	0.567
Basicity (mmol g^{-1})	0.019

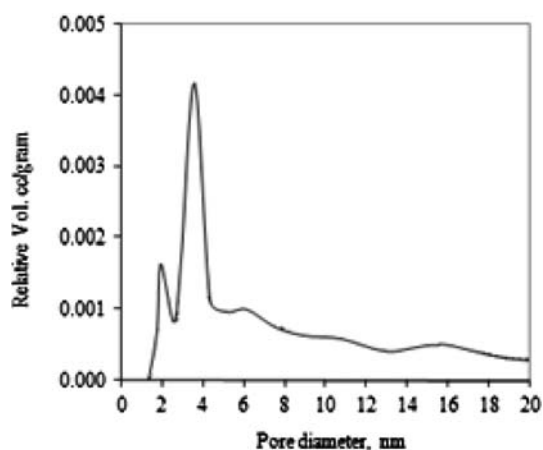


Fig. 1. Pore size distribution curve of carbon-coated monolith.

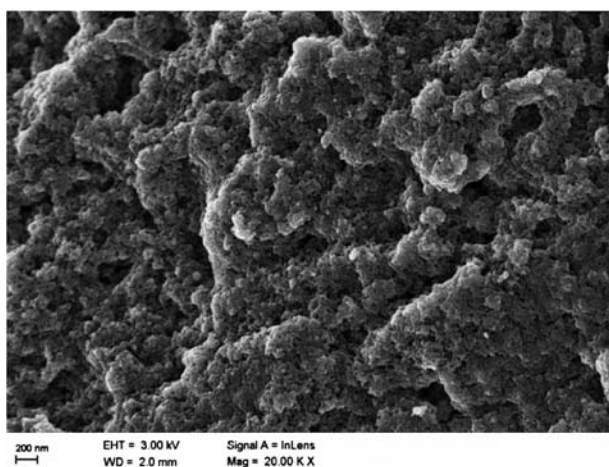


Fig. 2. SEM image of carbon-coated monolith.

Infrared spectrum of the adsorbent was recorded for two cases (before adsorption and after adsorption) in the range of $4,000\text{--}400 \text{ cm}^{-1}$ as presented in Fig. 4. Band assignments for the spectrum of carbon-coated monolith indicate that the carbonized carbon contains a number of atomic groups and structures such as OH, CH_2 , C=O, C–O–C, and so on. The most significant bands in the spectra of carbon-coated monoliths are those at range from 1,100 to 3,400. An overlapping of bands revealed between 800 and 1,200. A wide band at $3,420 \text{ cm}^{-1}$ can be ascribed to the presence of hydroxyl groups (OH stretch) due to carboxylic, phenolic, and the traces of water (not fully removed) in the KBr pellet. The absorption bands at $2,922 \text{ cm}^{-1}$ is assigned to hydrogen bonded to aliphatic carbon (ACH_2). A band at $1,620 \text{ cm}^{-1}$ is related with C=C stretching bond into aromatic rings. The band $1,178 \text{ cm}^{-1}$ can be described to the stretching vibration of the C–O bond related with C–O–H alcohols and C–O–C ether structures [25]. The spectrum of carbon-coated monolith shows the bands associated with cordierite structure such as Si–O, Mg–O, and Al–O are in the low wave number [26,27].

The changes in the FTIR of carbon-coated monolith were revealed by the elimination of oxygen and hydrogen atoms and the formation of new carbon–carbon bonds. Carbon of adsorbent is bonded with hydrogen atoms as attributed to vibration in alkanes and alkyl groups at $2,280 \text{ cm}^{-1}$. A band was observed at $1,620 \text{ cm}^{-1}$ before adsorption. After adsorption of MB onto carbon coated monolith, the band at $1,620 \text{ cm}^{-1}$ almost disappeared. This type of band is characterized for carbonaceous materials that were assigned to quinone-type carbonyl oxygen conjugated with the carbon basal plane present on carbon-coated monolith. The peaks between $1,550$ and $1,680 \text{ cm}^{-1}$ also suggested the quinone-type carbonyl. Quinine-

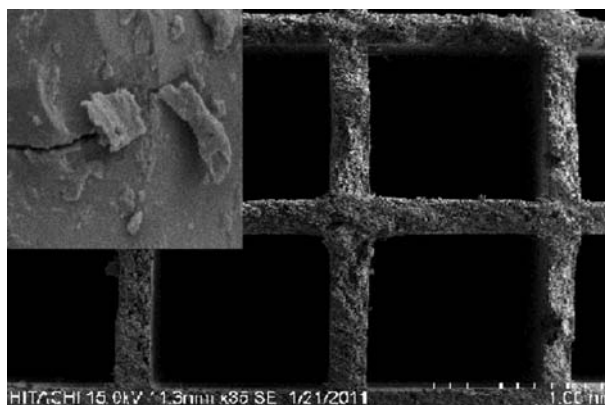


Fig. 3. SEM image of bare monolith.

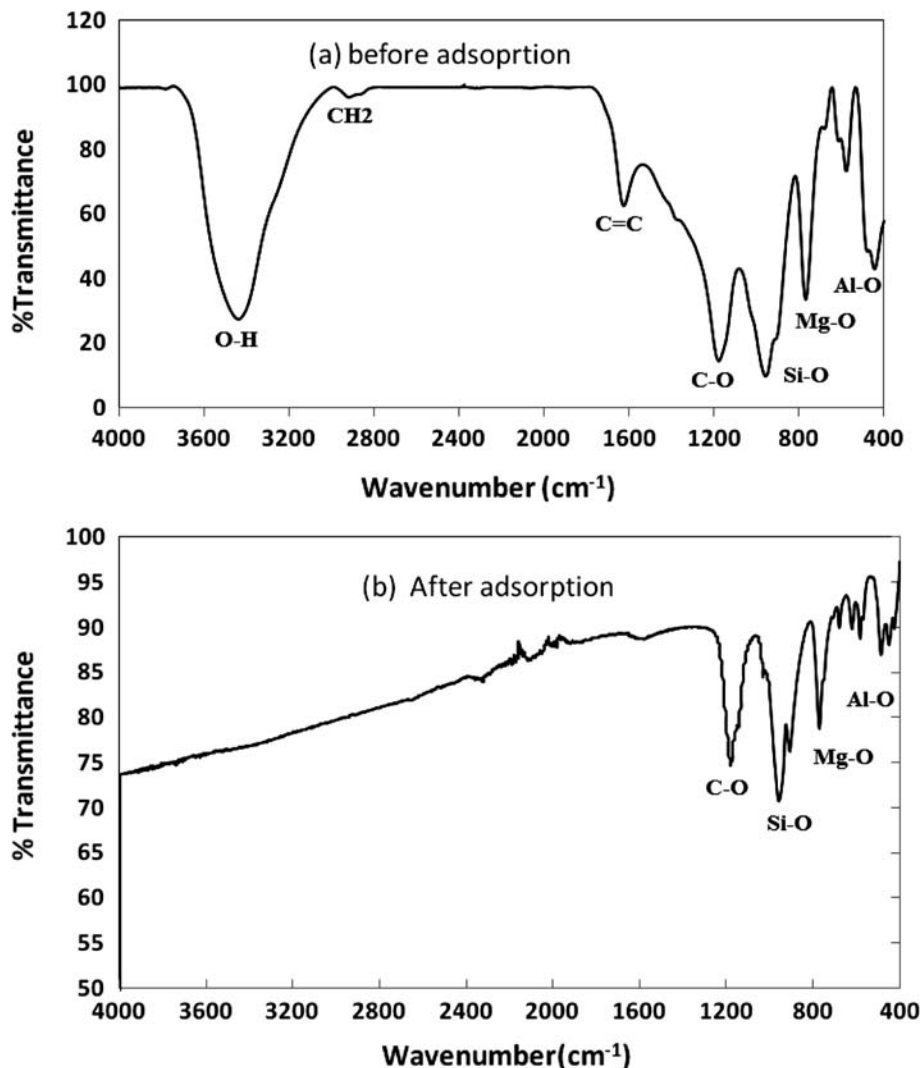


Fig. 4. FTIR patterns of carbon-coated monolith in the range of $4,000\text{--}400\text{ cm}^{-1}$ for (a) before adsorption, (b) after MB adsorption (temperature = 30°C , agitation speed = 150 rpm, and $C_0 = 480\text{ ppm}$).

type carbonyl and phenol groups provide the active sites for MB adsorption via electrostatic interaction. The OH band completely disappears due to MB adsorption. It is most likely that the hydrogen in OH group is involved in the formation of surface complex with intramolecular hydrogen bonding [25].

The surface chemical property of adsorbent was characterized by the Boehm's method. The amount of active sites was calculated based on some assumptions. The NaOH solution neutralizes carboxyl, lactone, and phenolic groups, Na_2CO_3 neutralizes carboxyl and lactone, NaHCO_3 neutralizes carboxyl groups, and HCl neutralizes all basic groups. The surface functional groups (active sites) analyzed by the Boehm titration are summarized in Table 1. The amount of acidic sites (0.567 mmol g^{-1}) is greater than that of basic sites

(0.019 mmol g^{-1}), suggesting that the majority of functional groups on the adsorbent surface are acidic.

3.2. Effect of pH

The pH of dye solution is one of the important factors controlling the adsorption process. The lowest adsorption was found to be at $\text{pH}=2$. The maximum adsorption was obtained at $\text{pH}=10$, illustrated in Fig. 5. Similar results of the pH effect were observed on MB adsorption [28]. Since MB is a cationic dye that it can be ionized in aqueous solution, it shows a positively charge chromophore. The electrostatic repulsion is caused by the positively charged surface sites on the adsorbent and the MB cations (MB^+) at lower pH. Thereby, the adsorption efficiency is relatively low

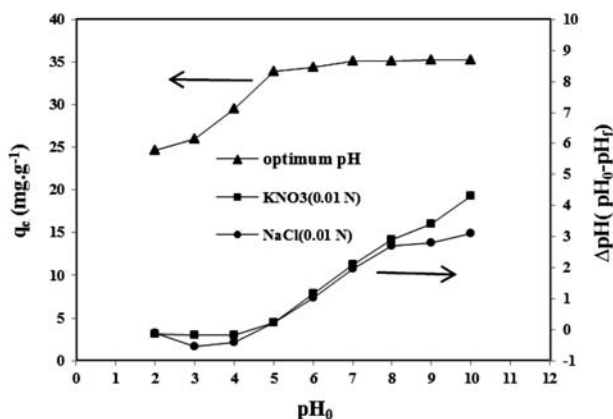


Fig. 5. Effect of pH ($C_0=100$ ppm) and point of zero charge (pH_{pzc}) of carbon-coated monolith using KNO_3 (0.01 N) and $NaCl$ (0.01 N) at $30^\circ C$, agitation speed = 150 rpm.

due to repulsion forces. At higher pH, the positively charged MB species and the negatively charged sites of adsorbent resulted in increasing attraction forces, thereby increasing the MB removal. The pH_{pzc} value was determined by the plotted curve. The point of intersection of the resulting curve with abscissa, at which $pH=0$, gave the pH_{pzc} as shown in Fig. 5. The pH_{pzc} was found to be 4.86, lower than the optimum $pH=10$. Cation adsorption is favored at pH higher than the pH_{pzc} , while anion adsorption is enhanced at pH less than pH_{pzc} [29].

3.3. Effect of contact time and initial concentration

Fig. 6 illustrates the adsorption of MB using different initial concentration 50, 80, 110, 140, 200, 300, 400, and 480 ppm at room temperature. The dye solution pH was kept constant at 10 by adding $NaOH$ (0.5 N) during the experiments. Carbon-coated monolith shows moderate ability to absorb MB from the aqueous solution. The adsorption kinetic was determined by analyzing the adsorptive uptake of MB aqueous solution at the different time intervals 5 min for 1 h and intervals 60 min for 5 h. Due to the availability of active sites, the adsorption was high during the initial period of the process. The adsorption process reached gradually to equilibrium with the decrease in adsorption sites due to occupation of MB with time. The percentage removal of MB decreased from 99.26% with an increase in initial dye concentration from 50 to 480 ppm. As the surface area of adsorptive sites is fixed, a high concentration of MB solution yielded lower efficiency of adsorption.

The BET surface area of adsorbents is an important factor in determining the adsorption capacities of the adsorbents while pore structures show an effective

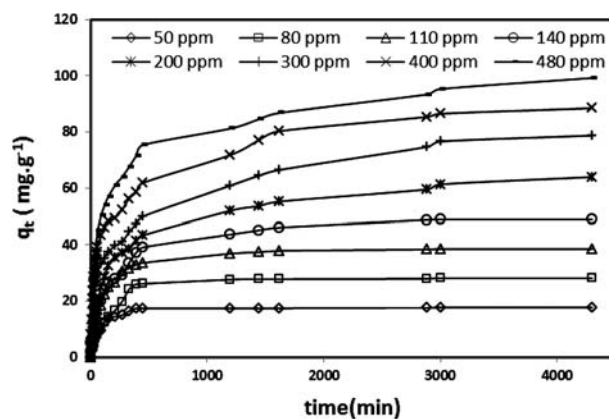


Fig. 6. Effect of contact time at various initial concentrations of MB on carbon-coated monolith, at $30^\circ C$, agitation speed = 150 rpm, and $pH=10$.

role in determining the adsorption capacity than the BET surface area. The adsorption on carbon-coated monolith may proceed through the steps, including diffusion from the bulk phase to the interior of the mesoporous and then to the micropores. With the presence of mesoporous, the path length of micropores for molecule migration into the carbon interior will be shortened, leading to an improved molecule transport. Indeed, mesoporous facilitate the access of adsorbate to the interior micropores.

3.4. Adsorption isotherm

The equilibrium isotherm theories describe the nature of coverage of adsorbate over an adsorbent surface and adsorbate–adsorbent interaction. Langmuir [30], Freundlich [31], Redlich–Peterson [31], and Dubinin–Radushkevich [32] isotherm models were used to study equilibrium data as shown in Table 2.

The isotherm parameters were calculated using the solver add-in with Microsoft's spreadsheet by minimizing the values of error function (the sums of squares error), and are listed in Table 2. The value of sums of squares error (SSE) was calculated as following:

$$SSE = \sqrt{\sum (q_{cal} - q_{exp})^2 / N} \quad (2)$$

The experimental data of equilibrium adsorption were compared to the isotherm models as shown in Fig. 7.

Obviously, the Redlich–Peterson model indicated the best fit of experimental data on the basis of the lowest value of SSE. However, the Langmuir model was also found to describe very well the experimental data. The essential characteristics of the Langmuir

equation can be expressed as a dimensionless factor namely R_L , as follows:

$$R_L = \frac{1}{1 + k_L C_0} \quad (3)$$

The value of R_L indicates that the type of isotherm to be irreversible ($R_L = 0$), favorable ($0 < R_L < 1$), linear ($R_L = 1$), and unfavorable ($R_L > 1$) [33]. The values of R_L are found to be in the range of 0.92–0.031, thus represent favorable adsorption. The R_L values were found to decrease as the concentration increase, indicating adsorption was more favorable to the lower concentrations. Table 3 show a comparison of the maximum monolayer absorption amount of MB on some adsorbents reported in the literature. Carbon-coated monolith prepared in this work has a moderate adsorption capacity of 121.3 mg g^{-1} . As a control, the bare monolith was found to have a very low adsorption capacity for MB (0.15 mg g^{-1}).

3.5. Kinetic studies

Selection of kinetic models depends on the nature of adsorbent, adsorption mechanism, and type of system. The pseudo-first-order model [35], pseudo-second-order model [36], Elovich [37], and intraparticle diffusion [38] were separately fitted to the experimental data. The linearized forms of the kinetic models are given in Table 4.

The plots of $\log(q_e - q_t)$ vs. t and t/q_t vs. t are presented in Figs. 8 and 9. The parameters α (adsorption rate) and β (desorption rate) are derived from the plots of q_t vs. $\ln(t)$. The adsorption rate was found to

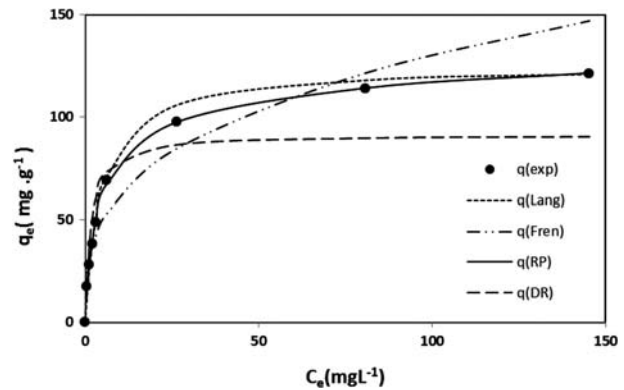


Fig. 7. Adsorption isotherm fitting to various models (temperature = 30°C , agitation speed = 150 rpm, and pH = 10).

increase with increasing the initial concentration whereas the desorption rates was found to decrease with increasing the initial concentration.

Table 4 presented the coefficients of the pseudo-first-order, second-order and Elovich models. The adsorption kinetics of MB for different initial concentrations were found to obey the pseudo-second-order kinetics, with high values of the correlation coefficient, r^2 (>0.98). In addition, the pseudo-second-order model showed $q_{e,cal}$ values closer to $q_{e,exp}$. From Table 4, it is found that the rate constant, k_2 , decreased from 1×10^{-3} to $4.8 \times 10^{-5} \text{ min}^{-1}$ for initial concentrations of MB ranging from 50 to 480 ppm. The driving force of diffusion is important for adsorption processes. The driving force changes with the dye concentration in bulk solution. An increase in the initial concentration provides an increase in the driving force to overcome all mass transfer resistances of the MB between the

Table 2
Isotherm models and the derived parameters of the models

Isotherms	Equation	Parameters	Value
Langmuir	$q_e = \frac{q_m k_L C_e}{1 + k_L C_e}$	q_m (mg g^{-1})	120.6
		k_L (L mg^{-1})	0.219
		SSE	3.977
Freundlich	$q_e = k_F C_e^{1/n}$	k_F ($\text{mg g}^{-1}(\text{L mg}^{-1})^{1/n}$)	35.68
		$1/n$	0.260
		SSE	8.938
Redlich-Peterson	$q_e = \frac{q_m k_{RP} C_e}{1 + k_{RP} C_e^\gamma}$	q_m (mg g^{-1})	84.36
		k_{RP} (L g^{-1})	0.401
		γ	0.923
		SSE	2.716
Dubinin-Radushkevich	$q_e = q_m \exp(-k_{DR}(RT \ln(1 + \frac{1}{C_e}))^2)$	q_m (mg g^{-1})	71.91
		k_{DR} (mol kJ^{-2})	0.0001
		SSE	29.47

Table 3
Adsorption capacities of various adsorbents

Adsorbent	pH	T (°C)	Maximum adsorption capacity (mg g ⁻¹)
Oil palm shell [34]	6.5	30	243.9
Meranti sawdust [28]	9	30	158.7
Bamboo dust [34]	7.2	30	143.2
Cedar sawdust [34]	–	20	142.3
Spent activated clay [28]	9.5	45	127.3
Carbon nanotube [20]	7	25	64.4
Luffa cylindria fibers [28]	–	30	49.9
Coir pith carbon [28]	6.9	35	5.87
This work	10	30	121.3

aqueous solution and carbon-coated monolith. The k_2 values indicated that the rate of adsorption was slower at higher initial MB concentration.

The rate-limiting step of the adsorption process was identified by using the intraparticle diffusion model. Fig. 10 presented the plot q_t vs. $t^{1/2}$ for different initial MB concentrations. The parameters were

summarized in Table 4. The plots presented multilinearity, indicating two or more steps occurred in the process. The flat part of plots demonstrates the gradual reduction of intraparticle diffusion due to equilibrium stage. Values of intercept give an idea about the thickness of boundary layer. The larger I value demonstrated a larger boundary-layer diffusion effect. The

Table 4
Parameters of kinetic models for MB adsorption onto CCM

C ₀ (ppm)	q _{exp} (mg g ⁻¹)	Pseudo-first-order			Pseudo-second-order		
		$\log(q_e - q_t) = \log q_e - \frac{k_1 t}{2.303}$ log(q _e - q _t) vs. t k ₁ × 10 ⁻⁴ (min ⁻¹)	q _{e,cal} (mg g ⁻¹)	r ²	$\frac{t}{q_t} = \frac{1}{k_2 q_e^2} + \frac{t}{q_e}$ $\frac{t}{q_t}$ vs. t k ₂ × 10 ⁻⁵ (mg g ⁻¹ min ⁻¹)	q _{e,cal} (mg g ⁻¹)	r ²
50	17.72	64.48	24.37	0.726	100	17.98	0.999
80	28.11	55.27	43.45	0.781	31	29.15	0.999
110	38.5	69.09	94.4	0.738	30	39.37	0.999
140	48.88	18.42	33.43	0.728	15	50.25	0.999
200	69.17	6.91	46.39	0.925	7.38	67.56	0.994
300	97.69	4.61	67.22	0.933	4.13	90.9	0.980
400	113.97	2.4	70.94	0.877	4.52	101.01	0.982
480	121.29	2.3	71.54	0.882	4.84	109.89	0.987

C ₀ (ppm)	q _{exp} (mg g ⁻¹)	Elovich			Intra-particle diffusion		
		$q_t = \frac{1}{\beta} \ln(\alpha\beta) + \frac{1}{\beta}(t)$ q _t vs. ln(t) α (mg g ⁻¹ min ⁻¹)	β (g mg ⁻¹)	r ²	$q_t = k_i t^{1/2} + I$ q _t vs. t ^{1/2} k _i (mg g ⁻¹ min ^{-1/2})	I (mg g ⁻¹)	r ²
50	17.72	3.37	0.237	0.953	0.848	1.60	0.726
80	28.11	5.34	0.161	0.933	0.937	2.29	0.781
110	38.5	6.96	0.127	0.965	1.483	3.26	0.738
140	48.88	7.74	0.116	0.970	1.606	5.06	0.728
200	69.17	9.39	0.097	0.976	1.658	12.69	0.925
300	97.69	9.44	0.096	0.944	1.714	15.38	0.933
400	113.97	11.73	0.079	0.935	1.943	21.96	0.877
480	121.29	14.05	0.067	0.953	2.457	24.27	0.882

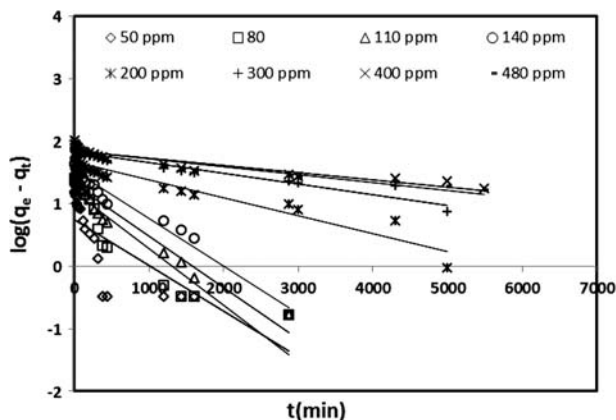


Fig. 8. Pseudo-first-order kinetics plot for the adsorption of MB at various concentrations onto carbon-coated monolith (temperature = 30 °C, agitation speed = 150 rpm, and pH = 10).

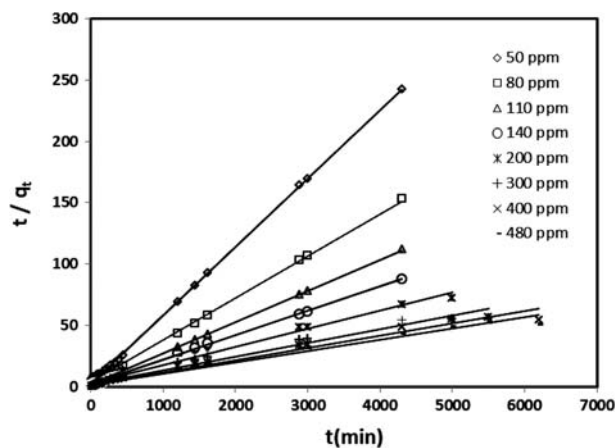


Fig. 9. Pseudo-second-order kinetics plot for the adsorption of MB at various concentrations onto carbon-coated monolith (temperature = 30 °C, agitation speed = 150 rpm, and pH = 10).

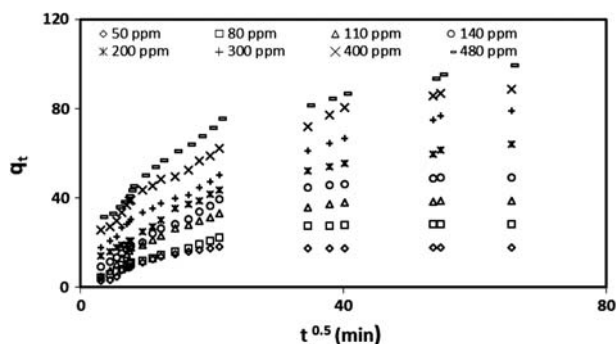


Fig. 10. Kinetic of MB adsorption at various concentrations using intraparticle diffusion model (temperature = 30 °C, agitation speed = 150 rpm, and pH = 10).

intercept value of plots increased (1.59–24.26 mg g⁻¹) with an increase in the initial concentration, indicating that high concentrations promoted the boundary layer diffusion effect.

3.6. Effect of temperature

The effect of temperature on the MB adsorption was investigated in the range of 30–50 °C. The results show the amount of MB adsorbed increased from 121.2 to 139.5 mg g⁻¹ when temperature increased from 30 to 50 °C. The free energy of adsorption, ΔG_0 , is determined using the equilibrium constant $K (= q_m k_L)$ values [39]:

$$\Delta G_0 = -RT \ln K \quad (4)$$

The magnitude of ΔH_0 and ΔS_0 may be determined using the relationship as given in Eq. (5):

$$\ln K = \frac{\Delta S_0}{R} - \frac{\Delta H_0}{RT} \quad (5)$$

The plot of $\ln K$ vs. $1/T$ is a straight line (Fig. 11), in which thermodynamic parameters ΔH_0 and ΔS_0 are obtained from the slope and intercept of the plot, respectively. The parameters are listed in Table 5. The negative values of ΔG_0 at 30–50 °C indicated that the

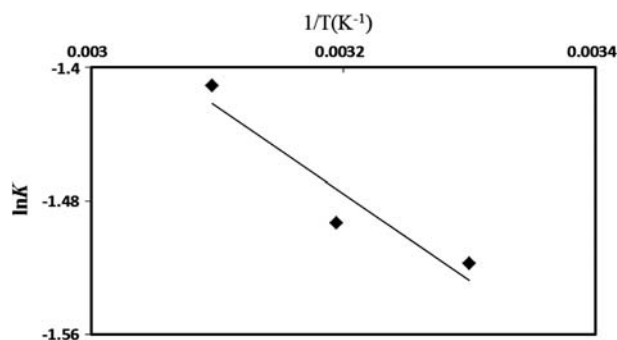


Fig. 11. Plot of $\ln K$ vs. $1/T$ of MB adsorption onto carbon-coated monolith at various temperature (agitation speed = 150 rpm, and pH = 10).

Table 5
Thermodynamic parameters for MB adsorption

Temperature (K)	ΔG_0 (kJ/mol)	ΔH_0 (J/mol)	ΔS_0 (J/mol)
303	-3.823		
313	-3.887	4,299	1.5
323	-3.789		

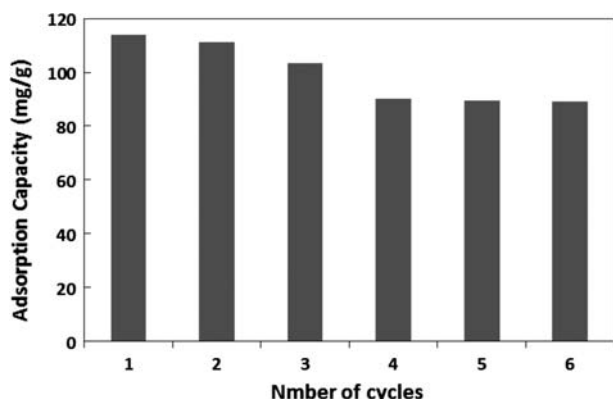


Fig. 12. Regeneration studies of CCM.

adsorption process was spontaneous. The positive values of ΔS_0 suggest the increased randomness at the solid/solution interface during the adsorption [40]. In the present study, the value of adsorption enthalpy change is less than 40 kJ mol^{-1} suggesting physical adsorption [41].

3.7. Regeneration studies

To study the reusability of carbon-coated monolith regeneration studies was carried out by batch process. Adsorption and desorption were repeated for six cycles and the results are shown in Fig. 12. The adsorption capacity of the monolith was found to reduce by about 20% after six cycles showing that the CCM can be reused without much loss in performance.

4. Conclusion

This paper presented the equilibrium study on the adsorption of MB onto carbon-coated monolith. Carbon-coated monolith showed high-surface area with majority pores in the mesoporous size. The FTIR result revealed a number of atomic groups that the majority of active sites are acidic. Hydroxyl and carboxyl groups are active site (acidic) in order to facilitate proton transfer. The honeycomb cordierite-based mesoporous carbons have mesopore texture with a wide pore size distribution having an average pore size of 4.0 nm. The wide pore size distribution is beneficial for the diffusion and adsorption of dyes of large molecule size, thus enhancing the adsorption efficiency of dye. The experiments data of MB adsorption are tested using two and three parameters isotherm models. Both Langmuir and Redlich-Peterson models describe well the equilibrium data. The pseudo-second-order model provided the best fitting of kinetic

data. The adsorption capacity of 121.3 mg g^{-1} shows that carbon-coated monolith can be considered as a promising material for MB removal. The adsorption capacity of the monolith was found to reduce by about 20% after six cycles.

Acknowledgments

The authors would like to gratefully acknowledge Universiti Putra Malaysia and MOHE (Project number: 03-04-10-803FR) for the financial support of this work.

Symbols

α	—	adsorption rate of Elovich, $\text{mg g}^{-1} \text{ min}^{-1}$
β	—	desorption rate of Elovich, g mg^{-1}
γ	—	Redlich-Peterson isotherm constant
C_0	—	Initial concentrations of dye solution, mg L^{-1}
C_t	—	concentrations of dye solution at time t , mg L^{-1}
C_e	—	concentrations of dye solution at equilibrium time, mg L^{-1}
I	—	thickness of the boundary layer, mg g^{-1}
k_i	—	constant rate of intraparticle diffusion, $\text{mg g}^{-1} \text{ min}^{-0.5}$
k_1	—	pseudo-first-order rate constant, min^{-1}
k_2	—	pseudo-second-order rate constant, $\text{mg g}^{-1} \text{ min}^{-1}$
k_F	—	Freundlich adsorbent capacity, $\text{mg g}^{-1} (\text{L mg})^{-1/n}$
k_L	—	Langmuir constant, L mg^{-1}
k_{DR}	—	equilibrium constant of Dubinin–Radushkevich model, $\text{mol}^2 \text{ kJ}^{-2}$
k_{RP}	—	constant rate of Redlich-Peterson, L g^{-1}
m	—	mass of adsorbent added to the solution, g
n	—	the reciprocal of reaction order
q_t	—	adsorption capacity at time t , mg g^{-1}
q_e	—	adsorption capacity at equilibrium conditions, mg g^{-1}
q_m	—	maximum adsorption capacity, mg g^{-1}
R_L	—	dimensionless group
R	—	gas constant
t	—	time, min
T	—	temperature, $^{\circ}\text{C}$
V	—	volume of the dye solution, L
ΔG_0	—	Gibb's free energy of adsorption, kJ mol^{-1}
ΔH_0	—	enthalpy of adsorption, J mol^{-1}
ΔS_0	—	entropy of adsorption, J mol^{-1}

References

- [1] O. Gerçel, H.F. Gerçel, A.S. Kopal, U.B. Oğutveren, Removal of disperse dye from aqueous solution by novel adsorbent prepared from biomass plant material, J. Hazard. Mater. 160 (2008) 668–674.

- [2] S. Karaca, A. Gurses, M. Acikyildiz, M. Ejder, Adsorption of cationic dye from aqueous solutions by activated carbon, Microporous Mesoporous Mater. 115 (2008) 376–382.
- [3] E. Blanca, E. Barragan, C. Costa, M. Carmen Marquez, Biodegradation of azo dyes by bacteria inoculated on solid media, Dyes Pigm. 75 (2007) 73–81.
- [4] L. Wang, J. Zhang, A. Wang, Removal of methylene blue from aqueous solution using chitosan-g-poly (acrylic acid)/montmorillonite super adsorbent nanocomposite, Physicochem. Eng. Aspects 322 (2008) 47–53.
- [5] I.M. Banat, P. Nigam, D. Singh, R. Marchant, Microbial decolorization of textile dye containing effluents, Bioresour. Technol. 58 (1996) 217–227.
- [6] S. Ledakowicz, M. Solecka, R. Zylla, Biodegradation, decolorisation and detoxification of textile wastewater enhanced by advanced oxidation processes, J. Biotechnol. 89 (2001) 175–184.
- [7] J.H. Mo, Y.H. Lee, J. Kim, J.Y. Jeong, Treatment of dye aqueous solutions using nanofiltration polyamide composite membrane for the dye wastewater reuse, Dyes Pigm. 76 (2008) 429–434.
- [8] A. Jumariah, T.G. Chuah, J. Gimbun, T.S.Y. Choong, I. Azni, Adsorption of basic dye onto palm kernel shell based activated carbon: Sorption equilibrium and kinetics studies, Desalination 186 (2005) 57–64.
- [9] C.H. Weng, Y.C. Sharma, S.H. Chu, Adsorption of Cr (VI) from aqueous solutions by spent activated clay, J. Hazard. Mater. 155 (2008) 65–75.
- [10] S.K. Nataraj, K.M. Hosamani, T.M. Aminabhavi, Nanofiltration and reverse osmosis thin film composite membrane module for the removal of dye and salts from the simulated mixtures, Desalination 29 (2009) 12–17.
- [11] M.S. Balathanigaimani, W.G. Shim, M.J. Lee, J.W. Lee, H. Moon, Adsorption isotherms of benzene and toluene on corn grain-based carbon monolith at 303.15, 313.15 and 323.15 K. J. Chem. Eng. Data, 53 (2008) 732–736.
- [12] M.J. Iqbal, M.N. Ashiq, Adsorption of dyes from aqueous solutions on activated charcoal, J. Hazard. Mater. 139 (2007) 57–66.
- [13] C.H. Weng, Y.F. Pan, Adsorption of a cationic dye (methylene blue) onto spent activated clay, J. Hazard. Mater. 144 (2007) 355–362.
- [14] A.P. Wang, F.Y. Kang, Z.H. Huang, Z.C. Guo, Preparation of porous carbons from halloysite–sucrose mixtures, Clay Min. 54 (2006) 485–490.
- [15] J. Li, J. Gu, H. Li, Y. Liang, Y. Hao, X. Sun, L. Wang, Synthesis of highly ordered Fe-containing mesoporous carbon materials using soft templating routes, Microporous Mesoporous Mater. 128 (2010) 144–149.
- [16] H. Yang, Z. Xu, M. Fan, R. Gupta, R.B. Slimane, A.E. Bland, I. Wright, Progress in carbon separation and capture: A review, J. Environ. Sci. 20 (2008) 14–27.
- [17] H. Muhammad, T.S.Y. Choong, T.G. Chuah, R. Yunus, T.Y.H. Yap, Adsorption of β carotene onto mesoporous carbon coated monolith in isopropyl alcohol and n-hexane solution: Equilibrium and thermodynamic study. Chem. Eng. J. 164 (2010) 178–182.
- [18] C.M. Castilla, A.F. Perez-Cadenas, Carbon-based honeycomb monoliths for environmental gas-phase applications, J. Mater. 3 (2010) 1203–1227.
- [19] Y. Yao, F. Xu, M. Chen, Z. Xu, Z. Zhu, Adsorption behavior of methylene blue on carbon nanotubes, Biores. Technol. 101 (2010) 3040–3046.
- [20] S. Hosseini, M. Ali Khan, M.R. Malekbala, W. Cheah, T.S.Y. Choong, Carbon coated monolith, a mesoporous material for the removal of methyl orange from aqueous phase: Adsorption and desorption studies, Chem. Eng. J. 171 (2011) 1124–1131.
- [21] M. Futamoto, U. Kawabe, H. Shigeyuki, Carbon fibers. JP patent, 78 (1978) 19 693.
- [22] D.S. Lafyatis, J. Tung, H.C. Foley, Poly (furfuryl alcohol)-derived carbon molecular sieves: Dependence of adsorptive properties on carbonization temperature, time, and poly (ethylene glycol) additives, Ind. Eng. Chem. Res. 30 (1990) 865–873.
- [23] L.S. Balistrieri, J.W. Murray, The surface chemistry of goethite (FeOOH) in major ion seawater, Am. J. Sci. 281 (1981) 788–806.
- [24] S.L. Goertzen, K.D. Theriault, A.M. Oickle, A.C. Tarasuk, H. A. Andreas, Standardization of the Boehm titration. Part I. CO₂ expulsion and endpoint determination, Carbon 48 (2010) 1252–1261.
- [25] C. Namasivayam, D.R. Kavitha, XRD and SEM studies on the mechanism of adsorption of dyes and phenols by coir pith carbon from aqueous phase, Microchem. J. 82 (2006) 43–48.
- [26] Y. Chen, Q. Chen, L. Song, H.P. Li, F.Z. Hou, Preparation and characterization of encapsulation of Europium complex into meso-structured silica monoliths using PEG as the template, Microporous Mesoporous Mater. 122 (2009) 7–12.
- [27] O.S. Bello, I.A. Adeogun, J.C. Ajalu, E.O. Fehintola, Adsorption of methylene blue onto activated carbon derived from periwinkle shells: Kinetics and equilibrium studies, Chem. Ecol. 2 (2008) 285–295.
- [28] D. Kavitha, C. Namasivayam, Experimental and kinetic studies on methylene blue adsorption by coir pith carbon, Bioresour. Technol. 98 (2007) 14–21.
- [29] E.C. Lima, B. Royer, J.C.P. Vagheti, N.M. Simon, B.M. Dacunha, F.A. Pavan, E.V. Benvenuti, R.C. Veses, C. Airoidi, Application of Brazilian-pine fruit coat as a biosorbent to removal of reactive red 194 textile dye from aqueous solution: Kinetics and equilibrium study, J. Hazard. Mater. 155 (2008) 536–550.
- [30] M.M. Nourouzi, T.G. Chuah, T.S.Y. Choong, Adsorption of glyphosate onto activated carbon derived from waste newspaper, Desalin. Water Treat. 24 (2010) 321–326.
- [31] Muhammad, T.G. Chuah, R. Yunus, A.R. Suraya, T.S.Y. Choong, Single and binary adsorption isotherm of Cd(II) and Zn(II) on palm kernel shell based activated carbon. Desalin. Water Treat. 29 (2010) 140–148.
- [32] P. Chakravarty, N. Sen Sarma, H.P. Sarma, Biosorption of cadmium (II) from aqueous solution using heartwood powder of Areca catechu, Chem. Eng. J. 162 (2010) 949–955.
- [33] I.D. Mall, V.C. Srivastava, G.V.A. Kumar, I.M. Mishra, Characterization and utilization of mesoporous fertilizer plant waste carbon for adsorptive removal of dyes from aqueous solution, Col. Surf. A: Physicochem. Eng. Aspects 278 (2006) 175–187.
- [34] I.A.W. Tan, A.L. Ahmad, B.H. Hameed, Enhancement of basic dye adsorption uptake from aqueous solutions using chemically modified oil palm shell activated carbon. Col. Surf. A: Physicochem. Eng. Aspects 318 (2008) 88–96.
- [35] S. Lagergren, About the theory of so called adsorption of soluble substances, Kungliga Svenska Vetenskapsakademiens, Handlingar, Band 24 (1898) 1–39.
- [36] Y.S. Ho, J.C.Y. Ng, G. McKay, Kinetics of pollutants sorption by biosorbents, Sep. Pur. Rev. 29 (2000) 189–232.
- [37] L. Ai, J. Jiang, R. Zhang, Uniform polyaniline microspheres: A novel adsorbent for dye removal from aqueous solution, Synth. Met. 160 (2010) 762–767.
- [38] T.W. Weber, R.K. Chakravorty, Pore and solid diffusion models for fixed bed adsorbers, American Ins. Chem. Eng. J. 20 (1974) 228–238.
- [39] Y. Bulut, H. Aydin, A kinetics and thermodynamics study of methylene blue adsorption on wheat shells, Desalination 194 (2006) 259–267.
- [40] V.S. Mane, I.D. Mall, V.C. Srivastava, Kinetic and equilibrium isotherm studies for the adsorptive removal of brilliant green dye from aqueous solution by rice husk ash, J. Environ. Manage. 84 (2007) 390–400.
- [41] S.K. Shukla, E.E. Ebenso, Corrosion inhibition, adsorption behavior and thermodynamic properties of streptomycin on mild steel in hydrochloric acid medium, Int. J. Electrochem. Sci. 6 (2011) 3277–3291.